JOURNAL OF RAMAN SPECTROSCOPY
J. Raman Spectrosc. 2005; **36**: 471–484
Published online in Wiley InterScience (www.interscience.wiley.com). DOI: 10.1002/jrs.1376

JRS

Surface-enhanced Raman sensors: early history and the development of sensors for quantitative biowarfare agent and glucose detection

Christy L. Haynes, Chanda Ranjit Yonzon, Xiaoyu Zhang and Richard P. Van Duyne*

Department of Chemistry, Northwestern University, 2145 Sheridan Road, Evanston, Illinois 60208-3113, USA

Received 14 November 2004; Accepted 12 April 2005

Surface-enhanced Raman spectroscopy (SERS) is a powerful technique for the sensitive and selective detection of low-concentration analytes. This paper includes a discussion of the early history of SERS, the concepts that must be appreciated to optimize the intensity of SERS and the development of SERS-based sensors. In order to achieve the lowest limits of detection, both the relationship between surface nanostructure and laser excitation wavelength, as well as the analyte/surface binding chemistry, must be carefully optimized. This work exploits the highly tunable nature of nanoparticle optical properties to establish the first set of optimization conditions. The SERS enhancement factor, EF_{SERS}, is optimized when the energy of the localized surface plasmon resonance (LSPR) lies between the energy of the excitation wavelength and the energy of the vibrational band of interest. With the narrow LSPRs used in this work, it is straightforward to achieve $EF_{SERS} \sim 10^8$. These optimization conditions were exploited to develop SERS-based sensors for two important target molecules: a *Bacillus anthracis* biomarker and glucose in a serum protein mixture. Using these optimized film-over-nanosphere surfaces, an inexpensive, portable Raman spectrometer was used successfully to detect the infectious dose of *Bacillus subtilis* spores with only a 5-s data collection. The biomarker used to detect the *Bacillus subtilis* spores binds irreversibly to SERS substrates, whereas other important biomolecules, such as glucose, do not have any measurable binding affinity to a bare silver surface. To overcome this difficulty, a biocompatible partition layer was self-assembled on the SERS substrate before exposure to the analyte solution. Using the partition layer approach to concentrate glucose near the SERS-active substrate, physiological glucose concentrations can be detected even in the presence of interfering serum proteins. Copyright © 2005 John Wiley & Sons, Ltd.

KEYWORDS: surface-enhanced Raman spectroscopy (SERS); history SERS discovery; localized surface plasmon resonance; SERS-based sensors

INTRODUCTION

In the 28 years since the discovery of surface-enhanced Raman spectroscopy (SERS),[1,2] this heretofore unknown spectroscopic phenomenon has progressed from model system studies of pyridine on a roughened silver electrode to state-of-the-art surface science studies[3–7] and then to real-world sensor applications[8–11] because: the required instrumentation has become smaller and cheaper;[12,13] and a myriad of materials and structures have been implemented successfully as SERS substrates.[4,7,14] Each year, the number of SERS publications increases as nanoscale materials design techniques advance and the importance of trace analyte detection increases. As a research group that has been studying SERS from the very beginning, we see as many exciting challenges ahead as stimulating results already achieved.

The electromagnetic enhancement mechanism is largely responsible for the enhancement of Raman scattering.[15] The magnitude of the electromagnetic enhancement is determined by the localized optical properties of nanoscale surface features. It is the intricate relationship between the surface structure and optical characteristics that determines the signal intensity. Both of these factors must be well controlled

*Correspondence to: Richard P. Van Duyne, Department of Chemistry, Northwestern University, 2145 Sheridan Road, Evanston, Illinois 60208-3113, USA.
E-mail: vanduyne@chem.northwestern.edu
Contract/grant sponsor: National Science Foundation;
Contract/grant numbers: DMR-0076097; CHE-0414554.
Contract/grant sponsor: Air Force Office of Scientific Research;
Contract/grant number: F49620-02-1-0381.
Contract/grant sponsor: Institute for Bioengineering and Nanoscience in Advanced Medicine.

to use SERS effectively. The conduction electrons in metal nanoparticles can be driven by light to oscillate collectively. This electron oscillation, also known as the localized surface plasmon resonance (LSPR), generates an electromagnetic field that is localized near the surface of a metal nanoparticle.[16] This large electromagnetic field induces a dipole in nearby molecules, thus enhancing Raman scattering from absorbed molecules. Surface-enhanced Raman spectroscopy is usually performed on Ag, Au or Cu[17,18] substrates because these metals have appropriate values of the real and imaginary parts of the dielectric constants[16] and can be handled easily in ambient, electrochemical and ultrahigh vacuum environments. Clearly, the choices of substrate material and excitation wavelength are the critical factors that affect the resulting enhancement factor. The work presented herein quantitatively demonstrates how the SERS enhancement factor, EF_{SERS}, depends on these characteristics.

In order to optimize EF_{SERS} and, accordingly, the analytical limit of detection (LOD), much effort has been devoted to substrate design. Early SERS substrates contained a random distribution of roughness feature sizes produced by oxidation–reduction cycling on a metal electrode[19] or evaporation of a thin metal film onto a flat substrate.[20] In recent years, researchers have explored the optimal size, shape, spacing and pattern of noble metal nanoparticles on surfaces. One of the most robust SERS substrates in use today is the metal film-over-nanosphere (MFON) substrate.[4,7,10] These substrates are simply fabricated by depositing a thin film (e.g. 200 nm) of Ag, Au or Cu onto a colloidal crystal assembly. The diameter of the colloidal nanosphere cores and the thickness of the metal film shell determine the size distribution of the roughness features and hence the optical response. Even though the nanoscale roughness features are not homogeneous in size, but instead are driven by the larger scale templating, they are homogeneous enough to generate a relatively narrow LSPR (full width at half-maximum, FWHM, ~200 nm). Recent experiments have demonstrated conclusively that MFON substrates are stable for months[11] (unlike many other nanostructured surfaces) and remain SERS-active even when exposed to large temperature[6] and potential excursions.[10] The utility of the MFON substrate is demonstrated herein as a robust SERS signal transduction agent used in biowarfare agent[11] and glucose detection.[8,9]

Although it is possible to fabricate stable Ag and Au substrates that yield large enhancement factors, the issue of surface generality still plagues SERS. In typical studies, the molecule of interest must reside at or near the nanoscale noble metal features. The utility of SERS would be enhanced greatly if the substrate could be made of any material (e.g. transition metals or catalytic materials) or if molecules that have no natural binding affinity for bare Ag, Au or Cu could be studied (e.g. glucose, ferrocene, etc.). Three approaches to surface generality have been developed. First, the range of substrate materials that can be used in SERS experiments was expanded significantly by decorating noble metal surfaces with thin (3–5 atomic layers) transition-metal films.[21,22] In fact, some groups have reported that by developing various procedures to roughen surfaces, synthesize nanoparticles and optimize the performance of confocal microscopes the weak SERS activity can be generated directly and observed from net transition metals (e.g., Pt, Ru, Rh, Pd, Fe, Co, Ni and their alloys).[23] In this case, the electromagnetic fields were damped but still strong enough to enhance Raman scattering. Second, decorating SERS-inactive surfaces such as gallium arsenide[24,25] and iron[26] with silver island films (3–8 nm) allowed adsorbates to be studied at the Ag/GaAs or Ag/Fe boundary. Finally, analyte can be dosed onto any surface and then probed by a SERS-active substrate mounted on a scanning probe microscopy tip.[27] This tip-enhanced Raman spectroscopy (TERS) approach holds great promise for the future.

HISTORICAL PERSPECTIVE ON THE DISCOVERY OF SERS

Before proceeding with the main themes of this paper, I (Van Duyne) have been asked by the editor of this special issue to provide some reflections on the very early history surrounding the discovery of SERS. Two disclaimers at the outset: these are my personal recollections and they have not been checked with others; and my apologies for the first-person style of this section and anything important I have forgotten to mention.

In the early 1970s it was clearly appreciated that the ability to observe vibrational spectra from a monolayer of molecules adsorbed on a solid surface would be a tremendous benefit in fields such as electrochemistry, heterogeneous catalysis and ultrahigh vacuum (UHV) surface science. Surface infrared spectroscopy was developing rapidly to fill this need. What about surface Raman spectroscopy? There seemed to be little chance because of the weakness of the Raman effect. Using an approach that I later documented in detail, I estimated that for one monolayer of a nonresonant adsorbate such as pyridine adsorbed in a vertical orientation on a platinum(111) single crystal and excited with 1 W of argon ion laser light at 488.0 nm, the total Raman signal for the 991 cm^{-1} fundamental integrated over the vibrational band would be something like 25 counts s^{-1} on a (then) state-of-the-art scanning double monochromator with a cooled photomultiplier tube as a detector.[28] I concluded that this experiment was just barely possible and therefore was of limited practicality. Subsequently I began to evaluate the options for enhancing the Raman signal. I evaluated three approaches: optimizing the performance of the Raman spectrometer; increasing the surface number density of Raman scatterers; and increasing the Raman scattering cross-section. The cross-section approach seemed likely to produce the best result and three methods were considered: choosing an adsorbate with the largest possible cross-section; employing near-ultraviolet, ultraviolet or even vacuum

ultraviolet laser excitation to take advantage of the fact that the cross-section scales with the fourth power of the laser frequency; and employing a laser excitation frequency deliberately chosen to coincide with an electronic transition in the adsorbate/metal system to take advantage of the resonance Raman effect. I chose to follow the resonance Raman approach even though I did not have a tunable dye laser at the time. I was hoping to find a suitable adsorbate with an electronic absorption spectrum that would overlap one of the argon ion laser lines.

In April 1974, I began the process of preparing a National Science Foundation research proposal describing our approach to obtaining the resonance Raman spectra of molecules adsorbed on electrode surfaces. Resonance Raman spectroscopy was known to have typical enhancement factors of 10^3–10^4 and I estimated that this would be enough to observe a signal with reasonable signal-to-noise ratio for one monolayer of resonant adsorbate on a single-crystal surface. Imagine my surprise in early May 1974 when I opened the May issue of *Chemical Physics Letters* and found the report by Fleischmann *et al*.[29] describing their observation of normal Raman signals from a monolayer of pyridine adsorbed on a roughened silver electrode immersed in a simple aqueous electrolyte solution in an electrochemical cell. I was stunned! They observed count rates of ~500–1000 counts per second using 100 mW of 514.5 nm argon ion laser light. Fleischmann *et al*. proved that the Raman signals were originating either from molecules directly adsorbed to the surface or very near the surface because they reversibly shifted in wavenumber and intensity with the applied electrode potential.

As luck would have it, I was scheduled to present a paper at the International Society of Electrochemistry meeting in Brighton, UK, in September 1974. After the meeting, I asked to visit Martin Fleischmann's laboratory at the University of Southampton. I was graciously received by Fleischmann and referred to Dr Jim McQuillan in the group for details on the Raman experiments. I was very keen to understand how it was possible to observe surface Raman signals from pyridine because I had just calculated how unlikely this experiment was to succeed. I learned from Jim that surface roughness was likely to be the key factor. In the past, Fleishmann had studied electrocrystallization phenomena in great detail and he knew that electrode surfaces such as that of silver became very rough after successive cycles of electrochemical oxidation in Cl^- (or other halide)-containing aqueous solutions to form AgCl crystallites that were reformed as silver metal islands upon reduction. Similarly, Pat Hendra had extensive experience in observing surface Raman spectra from pyridine adsorbed on high-surface-area Al_2O_3 or SiO_2 powders. Thus, it seemed clear enough that the surface area had been increased by several orders of magnitude so that many more pyridine molecules were being illuminated than at a flat smooth surface.

As I traveled back to Evanston a few weeks later, I realized that several important questions were left unanswered in the Fleischmann paper. These included:

1. Why was the Raman intensity of 500–1000 counts s^{-1} so high?
2. If the surface area was made ~1000 times greater, should not the double-layer capacitance of the electrode/solution interface have increased in proportion to the area, yielding a huge, easily measurable value of ~40 000 μF cm^{-2} ?

Furthermore, nothing unusual about the Raman process was noted in the paper. It was implied, but not stated, that this effect was ordinary normal Raman scattering from a high-surface-area material.

Upon my return to Northwestern University I prevailed on my outstanding graduate student, David Jeanmaire, to put his wonderful solution resonance Raman spectroelectrochemistry experiments on hold and attempt to repeat the Fleischmann experiments. Over the next two years David successfully repeated, and significantly extended, the Fleischmann experiments. In particular, we tested the hypothesis that surface roughening and increased surface area was the source of the increased Raman scattering. We reasoned that if we roughened the electrode more, the number of pyridine molecules adsorbed and hence the Raman signal should increase.

To test the surface area hypothesis, we repeated the Fleischmann electrochemical roughening procedure and carefully measured pyridine surface Raman intensity vs. the number of coulombs of charge passed. Surprisingly, we found that, starting from roughness conditions used by Fleischmann, the surface Raman signals *increased* as the surface roughness *decreased*! Eventually, we found that the 'optimum' level of roughness corresponded to the oxidation and re-reduction of approximately 100 monolayers of silver. On 5 February 1975 David Jeanmaire obtained Raman spectra of pyridine under mild roughening conditions that gave signals that were ~40 000 counts s^{-1} second with 200 mW of 514.5 nm laser light or ~10–20 times more intense than those reported by Fleischmann. Subsequently, David and I devised a procedure to measure the surface enhancement factor that compared the signal intensity per molecule on the surface to the signal intensity *per molecule* for the same molecule in free solution and discovered the 10^5–10^6 enhancement factor associated with SERS.[1,30] This result could not be explained by the surface area hypothesis. Two possibilities were considered to explain the enhancement: a 'hidden' resonance Raman enhancement or some new type of Raman enhancement mechanism. The resonance Raman explanation for the intensity disparity was described as 'hidden' because pyridine itself absorbs only at wavelengths shorter than ~280 nm, so it is not immediately apparent why one should expect a resonance enhancement mechanism to be operative at laser excitation wavelengths as long as 514.5 nm. We chose

to pursue the idea that a new type of Raman enhancement mechanism was operative.

The interesting task of speaking about and trying to publish these experiments came next. The discovery of these extremely intense surface Raman signals that resulted from optimizing the roughening procedure, electrolyte solution composition, applied potential, etc. was first reported publicly at an Electrochemical Society Meeting that had a symposium on 'Spectroscopic Methods in Electrochemical Studies'.[31] Fleischmann was the first speaker and he presented the studies reported in the 1974 paper[29] as well as other related work. I asked if he understood the origin of the intense Raman signals. As I remember it, he answered that the increased surface area was responsible for the observation. I was the second speaker and proceeded with my talk, entitled 'Resonance Raman spectroelectrochemistry', giving no hint that I would also talk about surface Raman spectroscopy. Near the end of this talk, I presented our results for the Raman spectroscopy of pyridine adsorbed on electrochemically roughened silver. The fact that our results could not be explained by the surface area hypothesis was immediately understood by the audience.

After the Electrochemical Society Meeting, I wrote a manuscript describing our results and sent it out for publication. The paper was rejected. I added some new results and tried submitting to another journal. It was rejected again. This process was repeated more times than I care to remember. Finally, I submitted our manuscript, which by now was rather long and contained surface Raman spectra for many molecules, electrode potentials, solution conditions, laser powers, etc., to the *Journal of Electroanalytical Chemistry* (received 7 October 1976). After an exhaustive review process, presumably due to the reluctance of reviewers to believe the unorthodox concept of surface enhancement, the paper was accepted (12 May, 1977) and subsequently published in November 1977.[1] The conclusions of this paper were:

1. The intensity of Raman scattering per pyridine molecule on electrochemically roughened Ag surfaces is 10^5–10^6 times greater than that from pyridine in solution.
2. All 27 normal modes of pyridine are observed and enhanced.
3. The surface Raman bands are depolarized.
4. A surface vibrational mode, assigned to the Ag–N stretch, was observed at 216 cm^{-1}.
5. All surface Raman bands show reversible potential dependence from 0.0 V vs. SCE $< E <$ −1.0 V vs. SCE.
6. The surface Raman intensity saturates for pyridine >50 mM. The ratio $[Cl^-]/[PYR] = 2.0$ optimizes the surface Raman intensity.
7. Heterocyclic amines, aromatic amines and some aliphatic amines show the surface enhancement effect.
8. For an adsorbate such as crystal violet, which absorbs strongly at the laser excitation wavelength, two enhancement processes contribute to the Raman intensity, the first being a surface enhancement effect identical to that of pyridine and the second a resonance Raman enhancement effect due to the coupling of the scattering process with an electronic transition in the adsorbed molecule.
9. A static double-layer electric field enhancement mechanism was postulated to explain the enhancement process observed for pyridine.

I also had an opportunity to attend a wonderful conference entitled 'Optics at the Solid–Liquid Interface' held near Nice, France, in May 1977. Two important benefits accrued from attending this meeting. First, I became acquainted with several physicists such as Andreas Otto, Tom Furtak and others who would begin my education on surface plasmons and later play extremely important roles themselves in the development of this new surface Raman spectroscopy. The proceedings of this conference were published and my paper 'Applications of Raman Spectroscopy in Electrochemistry', which covered both resonance Raman spectroscopy of electrochemically generated species in solution and surface Raman spectroscopy of adsorbates on roughened silver electrodes, appeared in October 1977.[30]

On 6 May 1977 I received a communication for review from the *Journal of the American Chemical Society* entitled 'Anomalously Intense Raman Spectra of Pyridine at a Silver Electrode' by M. G. Albrecht and Professor J. A. Creighton at the University of Kent. This short paper contained virtually identical results to those contained in the paper I had submitted to the *Journal of Electroanalytical Chemistry* in October 1976. In my naiveté as a young professor, I pointed out that the results of Albrecht and Creighton were so similar to those in our paper under review at the *Journal of Electroanalytical Chemistry* that I questioned the value of publication. The Albrecht and Creighton paper was published with great speed in July 1977.[2]

To bring this historical perspective to a close, it is clear in retrospect that Jeanmaire and I at Northwestern University and Albrecht and Creighton at the University of Kent independently demonstrated that the Raman signals associated with pyridine adsorbed on electrochemically roughened silver electrodes were indeed enhanced by a factor of 10^5–10^6. These two papers clearly showed that a new interaction between light and matter had been discovered. I attributed the enhancement to an increase in the electromagnetic field at the roughened surface, whereas Albrecht and Creighton hypothesized that resonance Raman scattering was responsible due to the creation of a charge-transfer absorption band between the adsorbate and the surface. These two ideas and their many refinements, the electromagnetic and chemical enhancement mechanisms, have dominated the mechanistic debate for 25 years. I named the phenomenon surface-enhanced Raman spectroscopy (SERS).[28]

It remains for the SERS community and perhaps also the wider scientific community to make the final determination on who discovered SERS.

EXPERIMENTAL

Chemicals

All chemicals used were of reagent grade or better. Silver (99.99%) was purchased from D.F. Goldsmith (Evanston, IL). Glass substrates 18 mm in diameter and no. 2 cover slips were from Fisher Scientific (Pittsburgh, PA). Pretreatment of substrates required H_2SO_4, H_2O_2 and NH_4OH, all of which were purchased from Fisher Scientific (Fairlawn, NJ). Oxygen-free high-conductivity copper was obtained from McMaster-Carr (Chicago, IL) and cut into 18-mm-diameter discs. Surfactant-free white carboxyl-functionalized polystyrene latex nanospheres of diameter (D) 390, 510, 600 and 720 nm were obtained from Duke Scientific Corporation (Palo Alto, CA) and Interfacial Dynamics Corporation (Portland, OR). Tungsten vapor deposition boats were purchased from R.D. Mathis (Long Beach, CA). Nitric acid (70%, Fisher Scientific), dipicolinic acid (2,6-pyridinedicarboxlic acid, DPA), calcium hydroxide, benzenethiol, 1,4-benzenedithiol and 3,4-dichlorobenzenethiol (Aldrich Chemical Co., Milwaukee, WI) were used as purchased. Water (18.2 $M\Omega cm^{-1}$) was obtained from an ultrapure filter system (Milli-Q, Millipore, Marlborough, MA). Compound $Fe(bpy)_3(PF_6)_2$ was synthesized as reported previously.[32] Calcium dipicolinate (CaDPA) was prepared from DPA and calcium hydroxide according to the method of Bailey and co-workers.[33] Bovine serum albumin (BSA), saline and TRIS buffer (pH 7.4) were obtained from Sigma (St. Louis, MO). The disposable filters with 0.45-μm-diameter pores were acquired from Gelman Sciences (Ann Arbor, MI). (1-Mercaptoundeca-11-yl) tri(ethylene glycol) ($HS(CH_2)_{11}(OCH_2CH_2)_3OH$, or EG3) was synthesized[34] and donated by the Mrksich group at the University of Chicago.

Spore samples

Bacillus subtilis was purchased from the American Type Culture Collection (Manassas, VA). Spore cultures were cultivated by spreading the vegetative cells on sterile nutrient agar plates (Fisher Scientific), followed by incubating at 30 °C for 6 days. The cultures were washed from the plates using sterile water and centrifuged at 12 000 *g* five times for 10 min each. The lyophilized spores were kept at 2–4 °C prior to use. Approximately 1 g of sample was determined to contain 5.6×10^{10} spores from optical micrographs (data not shown).

Nanosphere lithography and AgFON substrate fabrication

In this work, silver nanotriangles and AgFON substrates were fabricated on glass or copper substrates. Glass substrates were pretreated in two steps: piranha etch (*Caution*: piranha solution should be handled with great care) where H_2SO_4–30% H_2O_2 (3 : 1) at 80 °C for half an hour was used to clean the substrate; and base treatment where H_2O–NH_4OH–30% H_2O_2 (5 : 1 : 1) with sonication for 1 h was used to render the surface hydrophilic. Approximately 3 μl and 12 μl of nanosphere solution were drop-coated onto a clean glass and copper substrate, respectively, and allowed to dry at room temperature under ambient conditions. The metal films were deposited in a modified Consolidated Vacuum Corporation vapor deposition system with a base pressure of 10^{-6} Torr. The deposition rates for each film (3–10 Å s^{-1}) were measured using a Leybold Inficon XTM/2 quartz crystal microbalance (East Syracuse, NY). For nanosphere lithography substrates, the nanosphere mask was removed by sonication in absolute ethanol for 3 min, whereas the nanosphere mask was left intact for AgFON substrates. For glucose detection, AgFON substrates were incubated in 1 mM decanethiol or EG3 in ethanol for >12 h before use.

Plasmon-sampled surface-enhanced Raman excitation spectroscopy (PS SERES) apparatus

Spatially resolved extinction and SERS spectra were measured using a modified Nikon Optiphot (Frier Company, Huntley, IL) confocal microscope with a 20× objective in backscattering geometry. When recording an extinction spectrum, the tungsten–halogen microscope lamp provided white light excitation (the laser was blocked from entering the input fiber optic) and the output fiber optic was coupled to an Ocean Optics (Dunedin, FL) model SD2000 spectrometer. When recording a Raman spectrum, excitation was provided by one of the following lasers: Spectra-Physics (Mountain View, CA) model 2060 Ar^+ laser operating at an excitation wavelength (λ_{ex}) of 514.5 nm, Spectra-Physics model Millenia Vs laser operating at $\lambda_{ex} = 532.0$ nm or a Coherent (Santa Clara, CA) model 590 dye laser operating at $\lambda_{ex} = 632.8$ nm. In each case, the laser light was coupled into a 200-μm-core-diameter fiber using a Thorlabs (Newton, NJ) fiber launch, and appropriate Edmund Scientific (Barrington, NJ) interference filters and Kaiser (Ann Arbor, MI) holographic notch filters were placed in the beam path. For SERS spectra, the output fiber optic was coupled to an Acton (Acton, MA) VM-505 monochromator with the entrance slit set at 250 μm with a Roper Scientific (Trenton, NJ) Spec-10 : 400B liquid-N_2-cooled charge-coupled detector (CCD).

UV–Vis diffuse reflectance spectroscopy

Measurements were carried out using an Ocean Optics SD2000 spectrometer coupled to a reflection probe (Ocean Optics) and a halogen lamp (Model F-O-Lite H, World Precision Instruments, Sarasota, FL). The reflection probe consists of a tight bundle of 13 optical fibers (12 illumination fibers around a collection fiber) with a useable wavelength range of 400–900 nm. All reflectance spectra were collected against a mirror-like Ag film over glass substrate as the reference.

The SERS apparatus

A titanium–sapphire laser (model 3900, Spectra Physics, CW Ti : Saph) pumped by a solid-state diode laser (model Millenia Vs, Spectra Physics) was used to generate $\lambda_{ex} = 750$ nm. The SERS measurement system consists of an interference filter (Coherent), a holographic edge filter (Physical Optics Corporation), a single-grating monochromator with the entrance slit set at 100 μm (model VM-505, Acton Research Corporation), a liquid-N_2-cooled CCD (model Spec-10 : 400B, Roper Scientific) and a data acquisition system (Photometrics, Tucson, AZ). The spectral positions of the CCD pixels were calibrated using emission lines of known wavelengths from a Neon lamp. All the measurements were performed in ambient conditions.

A battery-powered portable Raman spectrometer[13] (model Inspector Raman, $\lambda_{ex} = 785$ nm) was purchased from DeltaNu (Laramie, WY) for the biowarfare agent sensor. For glucose detection, a Spectra-Physics model 120 HeNe laser was used to produce the 632.8 nm excitation wavelength. A small-volume flow cell[35] was used to control the external environment of AgFON surfaces throughout the SERS experiment.

Chemometrics method for glucose detection

All data processing was performed using MATLAB (MathWorks, Inc., Natick, MA) and PLS_Toolbox (Eigenvector Research, Inc., Manson, WA). Prior to analysis, cosmic rays were removed from the spectra using a derivative filter. The slowly varying background, commonly seen in SERS experiments, was removed mathematically by subtracting a fourth-order polynomial. This method minimally affected the SERS peaks while greatly reducing the background level. The SERS spectral intensities were normalized using the 1107 cm^{-1} peak from the EG3 partition layer spectrum before chemometric analysis. Then, data analysis was performed using leave-one-out (LOO) partial least-squares (PLS) analysis.

RESULTS AND DISCUSSION

In this work, we report fundamental and applied advancements in the field of SERS. The substrate optical properties are a pivotal consideration in all SERS experiments. Systematic studies of nanostructure optical properties and the resulting SERS enhancement factors yield general rules for maximizing SERS signals. With this in mind, the SERS signal transduction mechanism has been applied as both a biowarfare agent sensor to detect a biomarker for anthrax and as a medical diagnostic sensor to detect glucose.

Nanostructures with tunable LSPR optimized for SERS

As nanofabrication procedures have advanced, the roughness features on SERS substrates have become more homogeneous in size and shape. Early substrates, such as metal island films or aggregated colloids, contained a range of roughness features, contributing to a broad LSPR. Accordingly, a variety of different laser excitation wavelengths could be used to excite the LSPR and generate the large electromagnetic fields responsible for the SERS effect. However, it is unlikely that the maximum EF_{SERS} is achieved when only a portion of the nanoscale roughness features contribute to the SERS effect. To determine the largest possible ensemble-averaged EF_{SERS}, a small number of researchers performed wavelength-scanned surface-enhanced Raman excitation spectroscopy (WS SERES) experiments.[36–38] In the WS SERES experiment, the Raman-active molecule is adsorbed onto the substrate of choice and then the SERS spectrum of that adsorbate is captured using as many laser excitation wavelengths as possible. The intensity or enhancement factor of a specific Raman band is plotted versus the energy of the laser excitation to reveal the optimized experimental conditions. There are multiple difficulties in performing this important experiment: the number of data points in the WS SERES profile is limited by the number of laser excitation wavelengths available; if using a tunable laser to maximize the number of data points, signal is lost because a multi-stage monochromator is required to filter the Rayleigh scattering; and the information gained is only applicable to an adsorbate–substrate combination with exactly the same LSPR characteristics.

Recently, an alternative technique known as plasmon-sampled surface-enhanced Raman excitation spectroscopy (PS SERES)[3] was developed to explore the relationship between nanoparticle optics and the resulting EF_{SERS} while overcoming the deficiencies of the WS SERES technique. In the PS SERES experiment, the Raman-active molecule is adsorbed onto the substrate of choice, and then the correlated SERS and LSPR spectrum of that adsorbate are captured from a microscale domain using a single laser excitation wavelength. This procedure can be repeated on a single substrate until all the different LSPR domains have been sampled. The intensity or enhancement factor of a specific Raman band is plotted versus the LSPR maximum to reveal the optimized experimental conditions. There are multiple advantages in performing the PS SERES technique: the number of data points in the PS SERES profile is only limited by the number of microscale sample regions with different LSPR characteristics; the experiment requires only a single laser excitation wavelength, a single notch filter and a single-stage monochromator; and the information gained gives the general guidelines for achieving an optimized EF_{SERS} on any substrate with a narrow LSPR.

The SERS substrates used in the initial PS SERES experiments were silver nanoparticles produced using nanosphere lithography. These silver nanoparticles cover only 7% of the glass substrate and the size/shape can be tuned systematically by changing the nanosphere size in the deposition mask or the deposition thickness.[39,40] Slight variations in the size or shape of these nanoparticles yield

significant shifts in the narrow LSPR spectrum. For example, a 1-nm increase in the deposition thickness causes a 6-nm blue-shift in the LSPR λ_{max}.[40] Even though the structural variations among the nanoparticles on a given nanosphere lithography sample are small, they generate varying LSPR properties among microscale domains. In fact, the LSPR variation on a nanosphere lithography sample fits a Gaussian distribution with a standard deviation of ~10 nm[3]. Although it is possible to eliminate much of this variation if necessary, the PS SERES experiment exploits the distribution of optical properties to maximize the number of data points in the excitation profile. In all cases to date, PS SERES experiments have explored adsorbates that bind irreversibly to the silver nanoparticles in order to simplify data interpretation.

First, three separate PS SERES profiles were constructed using benzenethiol adsorbed onto silver nanoparticles; each profile was measured with a different laser excitation wavelength (514.5, 532.0 or 632.8 nm). The correlated LSPR and SERS spectra for the optimized enhancement factor in each case are shown in Fig. 1 and the PS SERES profiles are shown in Fig. 2. The profiles clearly demonstrate that the maximum enhancement factor occurs when the LSPR λ_{max} lies between the energy of the excitation wavelength and the vibrational mode (marked by the solid and dashed lines, respectively). It is interesting to note that the enhancement factor does not vary by more than a factor of ten once the signal is measurable above background. More PS SERES profiles were constructed with varied molecular adsorbates (3,4-dichlorobenzenethiol, 1,4-benzenedithiol and $Fe(bpy)_3^{2+}$) and similar results were

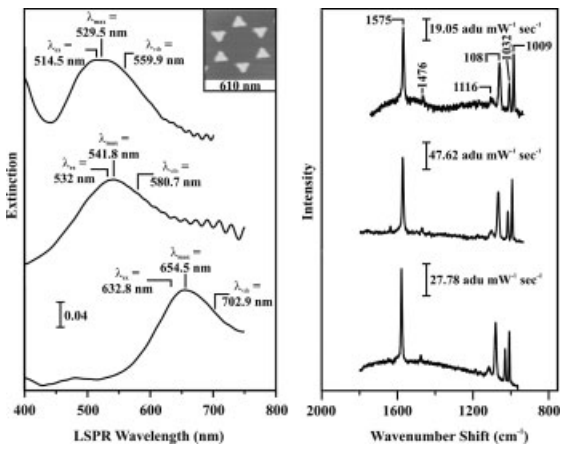

Figure 1. Correlated, spatially resolved LSPR and SERS spectra of benzenethiol-dosed nanosphere lithography substrates with maximized enhancement factors. (A) and (D) were measured from $D = 280$ nm, the mass thickness of Ag film (dm) = 36 nm, $P_{ex} = 0.7$ mW, $\lambda_{ex} = 514.5$ nm. (B) and (E) were measured from $D = 280$ nm, $d_m = 36$ nm, $P_{ex} = 0.7$ mW, $\lambda_{ex} = 532.0$ nm. (C) and (F) were measured from $D = 400$ nm, $d_m = 56$ nm, $P_{ex} = 1.2$ mW, $\lambda_{ex} = 632.8$ nm. All Raman spectra were captured with an integration time of 30 s.

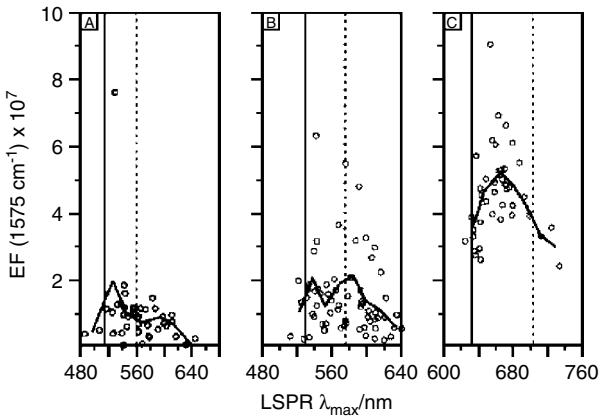

Figure 2. Plasmon-sampled SERES spectra for the ν_{8a} (1575 cm^{-1}) band of benzenethiol with three different excitation wavelengths: (A) $\lambda_{ex} = 514.5$ nm, (B) $\lambda_{ex} = 532.0$ nm, (C) $\lambda_{ex} = 632.8$ nm. For each λ_{ex}, both the wavelength location of the excitation (solid line) and the scattering (dashed line) are marked. The overlaid line represents the bin-averaged values of the LSPR λ_{max} and enhancement factor (EF).

achieved in all cases. The two non-resonant molecules yielded maximized enhancement factors of 2.3×10^7 and 1.4×10^8 whereas the maximum enhancement factor for the resonant molecule $Fe(bpy)_3^{2+}$ was 7.1×10^9. To verify that various vibrational modes adhere to the demonstrated pattern, PS SERES profiles were constructed for five different vibrational modes of 3,4-dichlorobenzenethiol, including in-plane ring deformations, a ring breathing mode, the C–S stretch and the C–C stretch. Again, the maximized enhancement factors occurred when the LSPR λ_{max} was between the excitation wavelength and the wavelength of the vibrational mode.

Thus, the PS SERES technique has revealed a general rule for optimizing EF_{SERS} when using substrates with narrow LSPR spectra. The largest EF_{SERS} is achieved when the energy corresponding to the narrow LSPR λ_{max} falls within a ~120 nm window that includes the energy of the excitation wavelength and the scattered photons. The LSPR variation on the nanosphere lithography substrates used in the work presented herein can be exploited easily to find the microscale domains with the best optical properties for a given experiment, thus maximizing the enhancement factor and lowering the detection limit. Although the reported enhancement factors are significantly smaller than those measured in single-molecule SERS studies,[41,42] these ensemble-averaged values can be achieved regularly and readily understood.

Optimization of SERS substrates for near-infrared laser excitation

For biological sensing applications, near-infrared (NIR) laser excitation is ideal because it reduces the native fluorescence

background from microorganisms. Additionally, NIR diode lasers are typically used as excitation sources in commercial, compact Raman spectrometers. In the study of *Bacillus* spore detection, we have used a CW Ti : Saph laser tuned to 750 nm as the laser excitation source to mimic a NIR diode laser.

As noted in the previous section, there is a strict correlation between the optical properties of SERS substrates and the scattering intensity with any given laser excitation wavelength. Like nanosphere lithography-fabricated nanotriangles, AgFON samples also exhibit a tunable LSPR that can be used to optimize the SERS signal by tuning the substrate LSPR wavelength to a value between that of the laser excitation (750 nm) and the vibrational band of interest (811 nm in the case presented below). Because AgFONs are not optically transparent, the reflectivity minimum (λ_{min}) was used to locate the LSPR maximum.

The extinction spectra were measured from a series of AgFON substrates with various nanosphere sizes using extinction spectroscopy measured in reflectance geometry in the visible region. Figure 3 shows the UV–Vis reflectance spectra of AgFON substrates with nanosphere diameters of 390, 510 and 600 nm. An AgFON sample was fabricated also using 720-nm-diameter spheres but the spectrum is not shown because the λ_{min} is shifted beyond the red limit (~900 nm) of the CCD. The reflectance spectrum of the AgFON with 600 nm diameter (D) and mass thickness of Ag film (d_m) of 200 nm shows the reflectivity minimum at 753 nm [Fig. 3(C)]. This substrate is expected to be the optimal SERS substrate for 750-nm laser excitation. In order to confirm this point, SERS spectra were measured from 1 mM benzenethiol on the AgFON substrates with D = 390, 510, 600 and 720 nm (Fig. 4). Benzenethiol was selected as a probe molecule because it is an efficient Raman scatterer. As depicted in Fig. 4, the largest enhancement of benzenethiol was observed from the AgFON with D = 600 nm and d_m = 200 nm. As expected, this follows the general guidelines established in the PS SERES experiment. Therefore, this AgFON substrate was selected as optimal for the *Bacillus* spore detection experiments that follow.

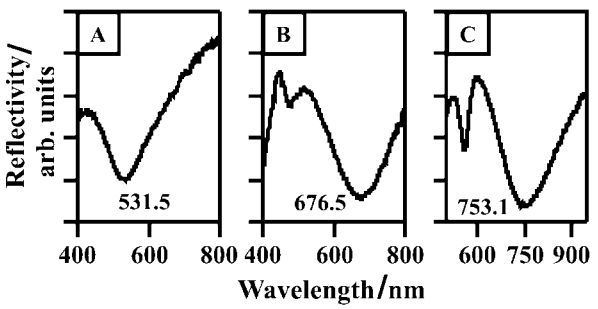

Figure 3. The UV–Vis diffuse reflectance spectra of different AgFON substrates in air: (A) D = 390 nm, d_m = 200 nm; (B) D = 510 nm, d_m = 200 nm; (C) D = 600 nm, d_m = 200 nm.

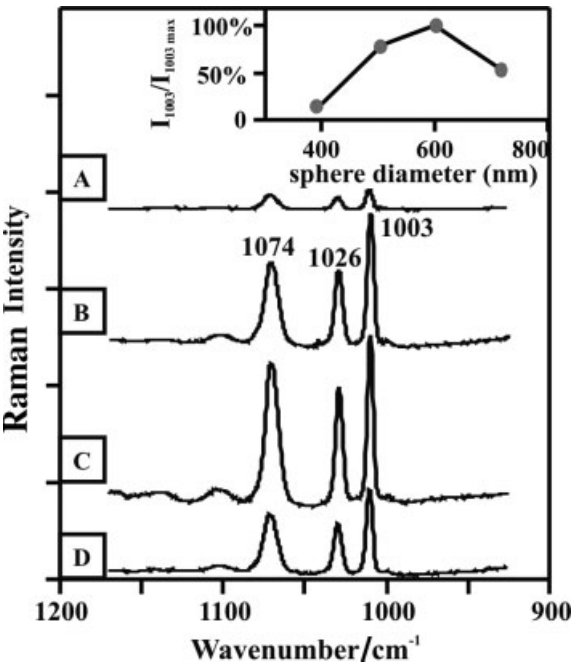

Figure 4. The SERS spectra of 20 µl of 1 mM benzenethiol in ethanol on different AgFON substrates: (A) D = 390 nm; (B) D = 510 nm; (C) D = 600 nm; (D) D = 720 nm. For all spectra λ_{ex} = 750 nm, P_{ex} = 3 mW, acquisition time = 1 min and d_m = 200 nm. The inset shows the variation of the Raman signal intensity at 1003 cm^{-1} with the sphere size.

Bacillus spore detection based on SERS

Surface-enhanced Raman spectroscopy has been exploited successfully in the rapid detection of *Bacillus subtilis* spores, which are harmless simulants for *Bacillus anthracis*. A *Bacillus* spore structurally consists of protective layers and a core cell. Calcium dipicolinate exists in these protective layers and can be used as the spore biomarker because other potentially interfering species do not contain this chemical.[43,44] Calcium dipicolinate was extracted from spores by sonicating in 0.02 M HNO_3 solution for 10 min. A 3.1×10^{-13} M spore suspension (3.7×10^4 spores in 0.2 µl of 0.02 M HNO_3) was deposited onto an AgFON substrate (D = 600 nm, d_m = 200 nm) for the SERS measurement. A high signal-to-noise ratio SERS spectrum was obtained in a 1-min data acquisition period [Fig. 5(A)]; this spectrum is dominated by bands associated with CaDPA [Fig. 5(B)], as seen in previous Raman studies on *Bacillus* spores.[45] The bands due to HNO_3 in the suspension were identified as well [Fig. 5(C)]. The peak at 1050 cm^{-1} in Fig. 5 is from the symmetrical stretching vibration of NO_3^-.[46,47] Because of its prominence, this band can be used as an internal standard to reduce the effect of intensity variations due to laser power fluctuations.

The SERS signal from extracted CaDPA was measured over the spore concentration range 10^{-14}–10^{-12} M to determine the saturation binding capacity of the AgFON surface and to calculate the adsorption constant (K_{spore} =

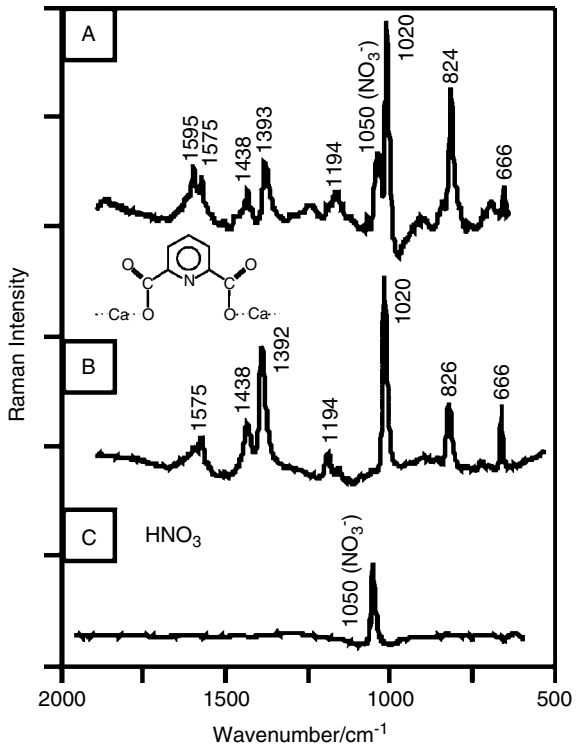

Figure 5. The SERS spectra of a 3.1×10^{-13} M spore suspension (3.7×10^4 spores in 0.2 µl of 0.02 M HNO_3) on AgFON substrate (A) and (B) 5.0×10^{-4} M CaDPA. (C) The SERS spectrum of 0.2 µl of 0.02 M HNO_3. For all spectra, $\lambda_{ex} = 750$ nm, $P_{ex} = 50$ mW, acquisition time = 1 min, $D = 600$ nm and $d_m = 200$ nm.

1.7×10^{13} M^{-1}). In Fig. 6(A) each data point represents the average intensity at 1020 cm^{-1} (a ring breathing mode) from three samples, with the standard deviation shown by the error bars. At low spore concentrations, the peak intensity increases linearly with concentration [Fig. 6(A) inset]. At higher spore concentrations, the response saturates as the adsorption sites on the AgFON substrate become fully occupied.

In order to monitor bioagent weapons or other harmful species, a SERS-based detection system must have the ability to detect less than the life-threatening dose of a pathogen in real or near-real time. Herein, the LOD is defined as the concentration of spores for which the strongest SERS signal of CaDPA at 1020 cm^{-1} is equal to three times the background SERS signal within a 1-min acquisition period. The background signal refers to the SERS intensity from a sample with a spore concentration equal to zero, which is theoretically predicted to be the intercept of the low concentration end of the spore adsorption isotherm [Fig. 6(A) inset]. Although lower detection limits can be achieved using longer acquisition times and higher laser power, the chosen parameters are reasonable for high-throughput, real-time and on-site analysis of potentially harmful species. The LOD for *B. subtilis* spores, evaluated by extrapolation of the linear concentration range of the adsorption isotherms [Fig. 6(A) inset], is found to be 2.1×10^{-14} M (2.6×10^3 spores in 0.2 µl of 0.02 M HNO_3). Furthermore, a similar spore concentration of 2.1×10^{-14} M was used to test the LOD prediction. A 1-min acquisition yields a SERS spectrum that clearly demonstrates

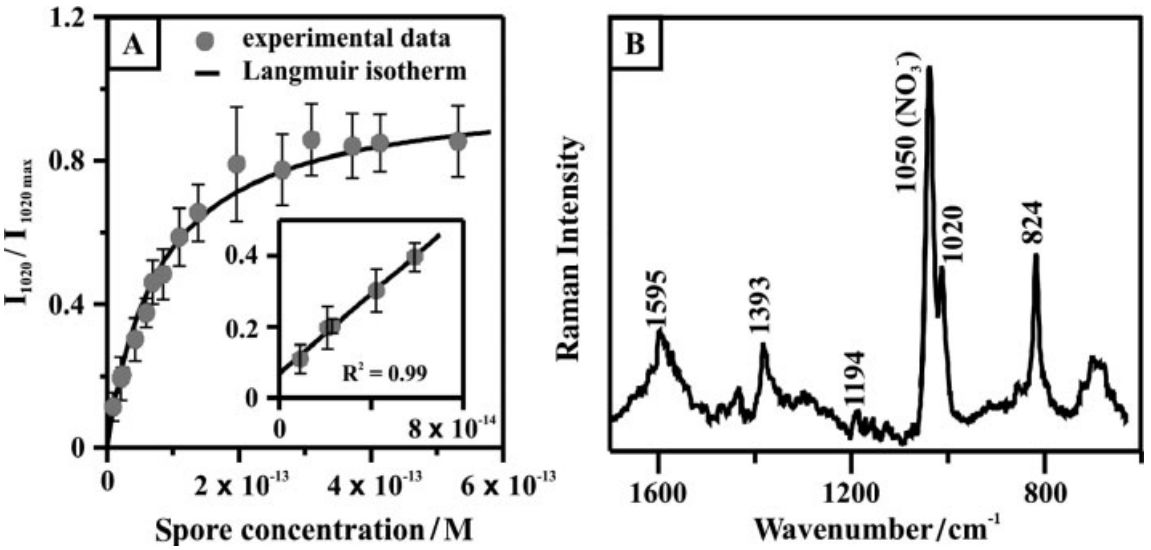

Figure 6. (A) Adsorption isotherm for *B. subtilis* spore suspension on an AgFON substrate. Intensity I_{1020} was taken from SERS spectra that correspond to varying spore concentrations in 0.2 µl of 0.02 M HNO_3 on AgFON substrates ($\lambda_{ex} = 750$ nm, $P_{ex} = 50$ mW, acquisition time = 1 min, $D = 600$ nm and $d_m = 200$ nm). A langmuir curve was generated with the adsorption constant for CaDPA from spores, $K_{spore} = 1.3 \times 10^{13}$ M^{-1}. The inset shows the linear range used to determine the LOD. Each data point represents the average value from three SERS spectra. Error bars show the standard deviations. (B) The SERS spectrum of a 2.1×10^{-14} M spore suspension (2.6×10^3 spores in 0.2 µl of 0.02 M HNO_3) on AgFON ($\lambda_{ex} = 750$ nm, $P_{ex} = 50$ mW, acquisition time = 1 min, $D = 600$ nm and $d_m = 200$ nm).

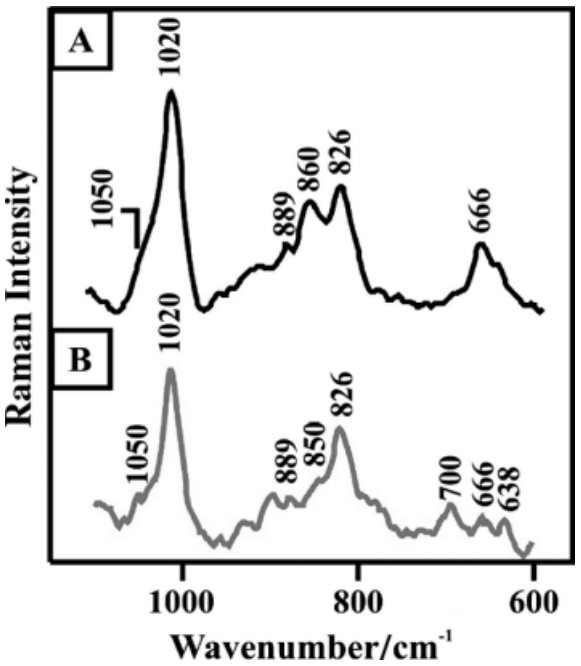

Figure 7. The SERS spectra obtained with a portable Raman spectrometer: (A) SERS spectrum of 8.3×10^{-14} M spore suspension (1.0×10^4 spores in 0.2 μl of 0.02 M HNO_3) on a 30-day-old prefabricated AgFON; (B) SERS spectrum of 10^{-4} M CaDPA in 0.2 μl of 0.02 M HNO_3 on a 30-day-old AgFON substrate ($\lambda_{ex} = 785$ nm, $P_{ex} = 35$ mW, acquisition time = 5 s, resolution = 15 cm^{-1}, $D = 600$ nm and $d_m = 200$ nm).

the spore Raman features [Fig. 6(B)] in comparison with Fig. 5(A). These data demonstrate that the SERS LOD is well below the anthrax infectious dose of 10^4 spores.[48]

Although SERS is a sensitive detection method for anthrax detection in the laboratory, many field-deployment applications require portability and flexibility that are challenging conventional laboratory-scale spectroscopic instrumentation.[43,49] Toward the goal of performing SERS detection of biowarfare agents in the field, a SERS spectrum of 10^4 *B. subtilis* spores dosed onto a 1-month-old AgFON substrate was readily acquired using a commercially available portable Raman instrument. A high signal-to-noise ratio spectrum was achieved within a data acquisition period of 5 s [Fig. 7(A)]. The SERS peak positions and intensity pattern for the spore sample are similar to those for the mixture of CaDPA and HNO_3 recorded utilizing the same device [Fig. 7(B)]. By coupling the portability and ease of use of this type of device with the molecular specificity and spectral sensitivity inherent to SERS, a range of possibilities are now open in the detection of harmful chemicals or bioagent weapons in real-world situations.

Glucose detection with SERS

Although the CaDPA biomarker in *B. subtilis* spores has an affinity toward the rough silver surface required for SERS detection, many important molecules (e.g. glucose) do not have any natural binding affinity for the silver surface.[8] The work presented herein demonstrates quantitative glucose detection by tailoring the SERS-active substrate with a self-assembled monolayer (SAM). All efforts to detect glucose on a bare AgFON surface using SERS were unsuccessful. Because the normal Raman cross-section of glucose should provide sufficient signal,[50] the inability to detect glucose using SERS must be attributed to the weak or non-existent binding of glucose to bare silver surfaces. To bring glucose within the range of the enhanced electromagnetic fields on the AgFON surface, a SAM can be formed on the surface to partition the analyte of interest (Fig. 8),[8] in a manner analogous to that used in high-performance liquid chromatography (HPLC).[22,51–54] Functionalizing the AgFON substrate with a partition layer has three advantages: the SAM stabilizes the Ag surface against oxidation; the SAM is exceedingly stable; and pre-concentration functionality is built in and tailorable by synthetic control of the partition layer.

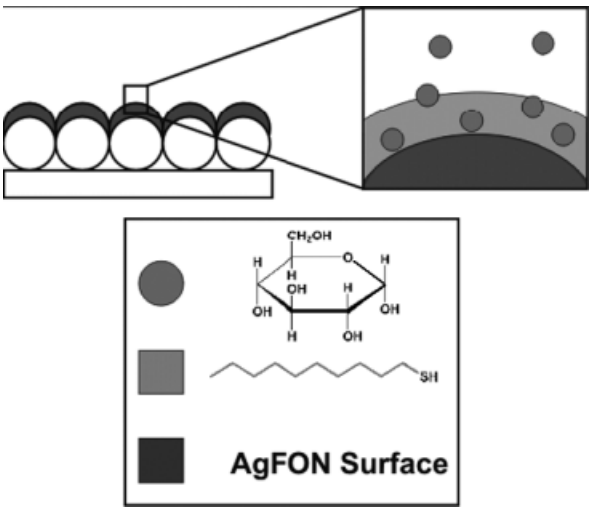

Figure 8. Schematic showing hypothetical glucose concentration gradient created by the 1-decanethiol partition layer.

In initial experiments, several SAMs were tested to determine their effectiveness as a partition layer. Of these, only the straight-chain alkanethiols were found to be effective partition layers, especially 1-decanethiol (1-DT), which forms a monolayer on Ag ~1.9 nm thick.[55] Fig. 9 shows example spectra from the different stages of assembly of the glucose/1-DT/AgFON surface. Figure 9(A) is the SERS spectrum of 1-DT on an AgFON surface. The substrate was then incubated in 100 mM glucose solution for 10 min and the SERS spectrum was collected [Fig. 9(B)]. This spectrum is the superposition of the SERS spectra for the partition layer and glucose. The SERS difference spectrum resulting from subtraction of spectrum 9A from spectrum 9B is shown in Fig. 9(C). The difference spectrum can be compared directly

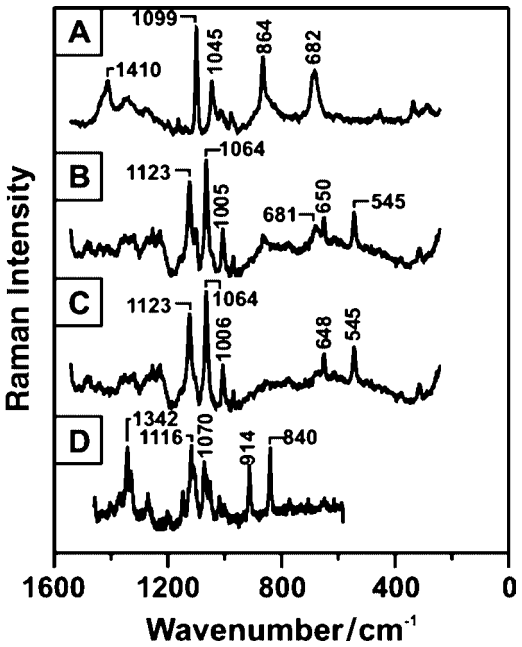

Figure 9. Spectra used in quantitative analysis: (A) 1-DT monolayer on AgFON substrate ($\lambda_{ex} = 532$ nm, $P = 1.25$ mW, acquisition time = 30 s); (B) mixture of 1-DT monolayer and glucose partitioned from a 100 mM solution ($\lambda_{ex} = 532$ nm, $P = 1.25$ mW, acquisition time = 30 s); (C) residual glucose spectrum produced by subtracting (A) from (B); (D) normal Raman spectrum of crystalline glucose for comparison ($\lambda_{ex} = 632.8$ nm, $P = 5$ mW, acquisition time = 30 s).

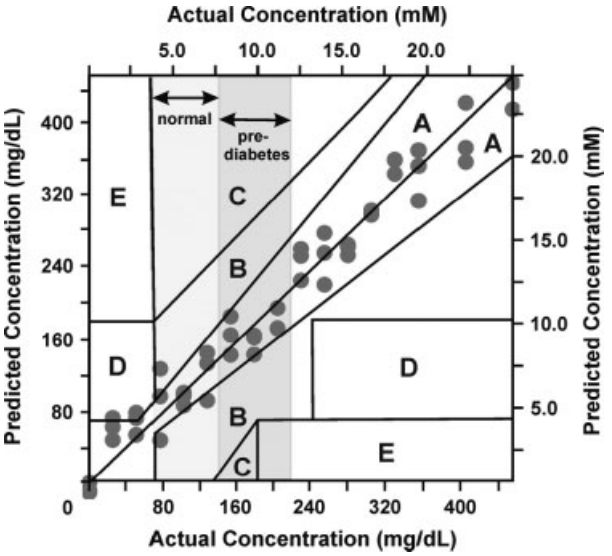

Figure 10. Clarke error grid of LOO-PLS predicted glucose concentration versus actual glucose concentration (five loading vectors). The AgFON samples were made ($D = 390$ nm, $d_m = 200$ nm), incubated for ~16 h in 1 mM EG3 solution and dosed in glucose solution (range: 0–450 mg dl^{-1}, 0–25 mM) for 10 min. Each SERS measurement was made in the flow cell under saline at pH 7.4 with $\lambda_{ex} = 632.8$ nm, $P_{laser} = 2.5$ mW and $t = 30$ s.

with the normal Raman spectrum of crystalline glucose shown in Fig. 9(D).

Although 1-DT was an effective partition layer for quantitative detection in the physiologically relevant concentration range (0–25 mM),[8] an ethylene glycol SAM was implemented in later experiments;[9] EG3 was chosen as a partition layer because of its ability to reject nonspecific binding by background proteins[56–59] and its biocompatibility,[60,61] progressing toward the long-term goal of fabricating an implantable glucose sensor. Each EG3-modified AgFON sample was incubated in saline solution with glucose (0–25 mM; 0–450 mg dl^{-1}) at a physiological pH of 7.4. Then, the samples were placed in an environmental control flow cell under saline and the SERS spectra were measured. The spectra were normalized using EG3 peak intensities, followed by LOO-PLS analysis. The resulting cross-validated glucose concentration predictions are presented in the Clarke error grid (Fig. 10).

Clarke *et al.*[62] established the Clarke error grid as the metric for evaluating glucose sensor efficacy in the clinical concentration range. The Clarke error grid is divided into five major zones: zone A predictions lead to clinically correct treatment decisions; zone B predictions lead to benign errors or no treatment; zone C predictions lead to overcorrection of acceptable blood glucose concentrations; zone D predictions lead to dangerous failure to detect and treat; and zone E predictions lead to further aggravation of abnormal glucose levels.

The EG3-modified AgFON sensor allows quantitative detection of glucose in the physiological range with a corresponding prediction error of 82 mg dl^{-1} (4.5 mM). In Fig. 10, 94% of the predictions fall in zones A and B whereas only a few data points overlap in zone D within the hypoglycemic area (<70 mg dl^{-1}, <3.9 mM). The error of 82 mg dl^{-1} (4.5 mM) can be attributed partially to variation of EF_{SERS} on different AgFON samples. The nanostructure on an AgFON substrate varies from point to point, affecting the localized surface plasmon resonance and, accordingly, EF_{SERS}. Figure 11 clearly demonstrates the improved prediction error when all SERS measurements are recorded from a single spot on an AgFON substrate.

Although quantitative detection is an important characteristic of a viable biosensor, the glucose sensor also must be effective in the presence of interfering proteins. Bovine serum albumin was used as a blood serum protein mimic to challenge the glucose sensor. The EG3-functionalized AgFON substrate was placed in a flow cell in a saline environment and the SERS spectrum was obtained [Fig. 12(A)]. Then, the BSA solution was injected into the flow cell and the SERS spectrum was collected throughout the 240-s incubation [Fig. 12(B)]. Finally, the sample was exposed to 100 mM glucose and the SERS spectrum was collected [Fig. 12(C)]. Figure 12(D) is the difference spectrum demonstrating that

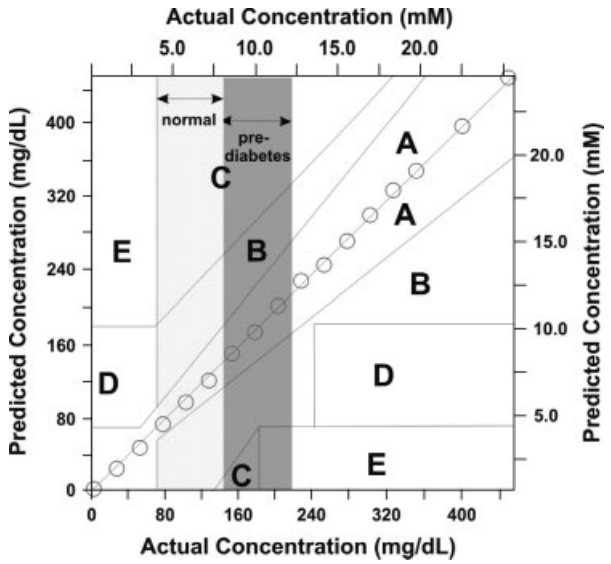

Figure 11. Clarke error grid of LOO-PLS predicted glucose concentration versus actual glucose concentration (three loading vectors). The AgFON samples were made ($D = 390$ nm, $d_m = 200$ nm), incubated for ~16 h in 1 mM EG3 solution and dosed in glucose solution (range: 0–450 mg dl^{-1}, 0–25 mM) for 10 min. Each SERS measurement was made in the flow cell under saline at pH 7.4 with $\lambda_{ex} = 632.8$ nm, $P_{laser} = 1.0$ mW and $t = 30$ s. All the SERS measurements were done in a single spot.

BSA does not have a measurable SERS spectrum. The lack of SERS BSA bands could be due to inefficient adsorption of BSA to the EG3 partition layer. Figure 12(E) demonstrates that the SERS glucose sensor is still effective after substrate exposure to an interfering protein and that the peaks correspond to the crystalline glucose peaks shown in Fig. 12(F). This experiment clearly shows that glucose partitioning into EG3 is not influenced by the presence of large molecules such as BSA. It is interesting to note that the peak at 695 cm^{-1} [Fig. 12(A)] shifts to 710 cm^{-1} [Fig. 12(C)] in the presence of glucose. The rearrangement of the SAM when the glucose molecules partition into EG3 may cause this shift. The observed shift further supports the hypothesis of glucose penetrating deeply into the EG3 monolayer, affecting even the character of the C–S bond.

In addition to demonstrating quantitative glucose detection in a clinically relevant concentration range and detection of glucose in the presence of other interfering proteins, other characteristics of the EG3-modified AgFON glucose sensor, such as durability and reusability, are demonstrated in published work.[9]

CONCLUSION

This paper details two major advances: the development of a general rule for optimizing EF_{SERS} on nanofabricated substrates with narrow localized surface plasmon resonances; and the exploitation of these optimized SERS substrates for environmental and biomedical sensing applications.

The optical properties of the SERS substrate play a key role in achieving the largest possible value of EF_{SERS}. The general guidelines established in this work exploit the narrow LSPRs and optical tunability of nanosphere lithography-fabricated nanoparticles, however the conclusions can be applied to any SERS substrate that has a narrow LSPR. The largest EF_{SERS} is observed when the energy corresponding to the LSPR λ_{max}, measured by extinction spectroscopy in transmission geometry, falls within a ~120 nm window that includes the energy of the excitation wavelength and the Stokes-shifted Raman output photons. This protocol can be extended to AgFON substrates. Although AgFONs have a broader LSPR, the highest enhancement is, indeed, attained when the LSPR λ_{min}, measured by extinction spectroscopy in reflectance geometry, lies between the excitation wavelength and the scattering wavelength.

The SERS signal transduction mechanism has many characteristics that can be exploited in biosensing applications: sensitivity, selectivity and no interference from water molecules. Optimized SERS substrates with maximized enhancement factors yield lower detection limits. Herein, the optimized AgFON substrate is applied to detect quantitatively two important analytes: a biomarker for anthrax, and glucose.

This work details the development of a rapid detection protocol suitable for use by first-responders to detect *Bacillus* spores using a low-cost, battery-powered, portable Raman spectrometer. Calcium dipicolinate, a biomarker for *Bacillus* spores, was efficiently extracted from spores by sonication in nitric acid and rapidly detected using SERS. The SERS signal from extracted CaDPA was measured over the spore concentration range of 10^{-14}–10^{-12} M to determine the adsorption capacity of the AgFON surface for CaDPA and to calculate the adsorption constant ($K_{spore} = 1.7 \times 10^{13}$ M^{-1}). At present, an 11-min procedure is capable of achieving a LOD of $\sim 2.6 \times 10^3$ spores, which is below the anthrax infectious dose of 10^4 spores. This sensing modality has been transitioned successfully from a laboratory spectrometer to a field-portable instrument, where 10^4 *Bacillus* spores can be detected with a 5-s data acquisition period on a 1-month-old AgFON substrate.

Unlike CaDPA, glucose does not have any natural binding affinity toward a bare silver surface. To overcome this problem, EG3 was self-assembled on the AgFON surface to partition the glucose, bringing it within range of the enhancing electromagnetic fields. The work reviewed herein demonstrates quantitative glucose detection in the physiological range (0–450 mg dl^{-1}; 0–25 mM) under physiological pH. Over 94% of the data fall in zones A and B in the Clarke error grid, making the SERS sensor a viable technique for the clinical measurement of glucose. Additionally, to demonstrate the utility of the SERS glucose sensor in the presence of protein interferants, glucose was detected quantitatively

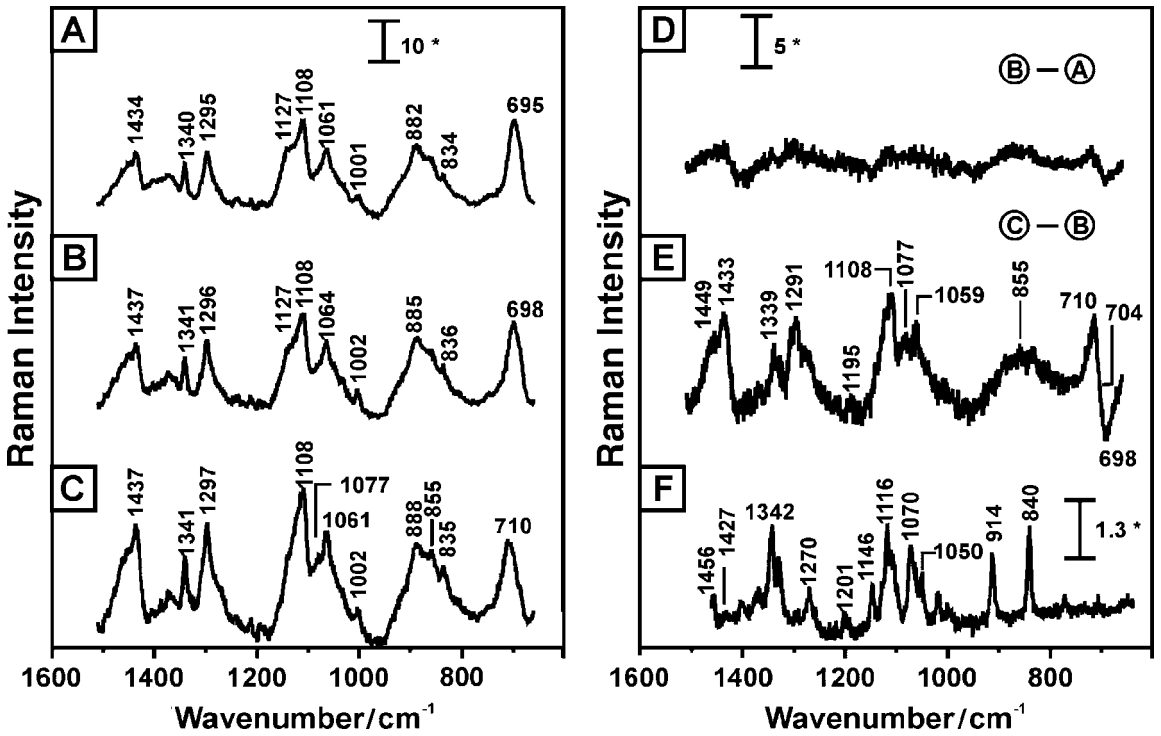

Figure 12. Six SERS spectra showing detection of glucose in the presence of bovine serum albumin (BSA): (A) EG3 monolayer on AgFON substrate ($\lambda_{ex} = 632.8$, $P_{laser} = 0.8$ mW, $t = 240$ s); (B) 1 mg ml^{-1} BSA injected into the flow cell to challenge the EG3-modified AgFON ($\lambda_{ex} = 632.8$, $P_{laser} = 0.8$ mW, $t = 240$ s); (C) 100 mM glucose injected into the flow cell ($\lambda_{ex} = 632.8$, $P_{laser} = 0.8$ mW, $t = 240$ s); (D) difference spectrum obtained by subtracting (A) from (B), revealing the lack of SERS spectrum for adsorbed BSA; (E) difference spectrum obtained by subtracting (B) from (C), indicating that BSA exposure does not interfere with glucose detection; (F) normal Raman spectrum of crystalline glucose for comparison ($\lambda_{ex} = 632.8$, $P_{laser} = 5$ mW, and $t = 30$ s; * denotes adu mW^{-1} s^{-1}).[50]

in a mixture including serum albumin, the most abundant protein in plasma.

The use of optimized SERS substrates offers unique analytical features for the analysis of anthrax and glucose, as well as many other potential targets. With the appropriate surface modification, any Raman-active molecule can be detected quantitatively at the trace level in near-real-time using SERS as the signal transduction mechanism. The speed and sensitivity of SERS make this method a viable option for the field analysis of potentially harmful environmental samples and *in vivo* monitoring of blood glucose levels.

Acknowledgements

This work was supported by the National Science Foundation (DMR-0076097, CHE-0414554), the Air Force Office of Scientific Research MURI program (F49620-02-1-0381), the Institute for Bioengineering and Nanoscience in Advanced Medicine (IBNAM) at Northwestern University, a Northwestern University Presidential Fellowship (C.L.H.) and a Northwestern University MRSEC Fellowship (X.Z.).

REFERENCES

1. Jeanmaire DL, Van Duyne RP. *J. Electroanal. Chem.* 1977; **84**: 1.
2. Albrecht MG, Creighton JA. *J. Am. Chem. Soc.* 1977; **99**: 5215.
3. Haynes CL, Van Duyne RP. *J. Phys. Chem. B.* 2003; **107**: 7426.
4. Jensen TR, Van Duyne RP, Johnson SA, Maroni VA. *Appl. Spectrosc.* 2000; **54**: 371.
5. Dick LA, Haes AJ, Van Duyne RP. *J. Phys. Chem. B.* 2000; **104**: 11 752.
6. Litorja M, Haynes CL, Haes AJ, Jensen TR, Van Duyne RP. *J. Phys. Chem. B.* 2001; **105**: 6907.
7. Dick LA, McFarland AD, Haynes CL, Van Duyne RP. *J. Phys. Chem. B.* 2002; **106**: 853.
8. Shafer-Peltier KE, Haynes CL, Glucksberg MR, Van Duyne RP. *J. Am. Chem. Soc.* 2003; **125**: 588.
9. Yonzon CR, Haynes CL, Zhang X. *Anal. Chem.* 2004; **76**: 78.
10. Zhang X, Yonzon CR, Van Duyne RP. *Proc. SPIE-Int. Soc. Opt. Eng.* 2003; **5221**: 82.
11. Zhang X, Young MA, Lyandres O, Van Duyne RP. *J. Am. Chem. Soc.* 2005; **127**: 4484.
12. Young MA, Stuart DA, McFarland AD, Lyandres O, Glucksberg MR, Van Duyne RP. *Can. J. Chem.* 2004; **82**: 1435.
13. www.deltanu.com [July 2004].
14. Vo-Dinh T, Stokes DL, Griffin GD, Volkan M, Kim UJ, Simon MI. *J. Raman Spectrosc.* 1999; **30**: 785.
15. Schatz GC, Van Duyne RP. *Electromagnetic Mechanism of Surface-Enhanced Spectroscopy*, vol. 1. John Wiley: New York, 2002; 759.
16. Kreibig U, Vollmer M. *Optical Properties of Metal Clusters*, vol. 25. Springer-Verlag: Heidelberg, 1995; 532.
17. Siemes C, Bruckbauer A, Goussev A, Otto A, Sinther M, Pucci A. *J. Raman Spectrosc.* 2001; **32**: 231.
18. Graff M, Bukowska J, Zawada K. *J. Electroanal. Chem.* 2004; **567**: 297.

19. Stacy AM, Van Duyne RP. *Chem. Phys. Lett.* 1983; **102**: 365.
20. Kovacs GJ, Loutfy RO, Vincett PS, Jennings C, Aroca R. *Langmuir* 1986; **2**: 689.
21. Park S, Yang P, Corredor P, Weaver MJ. *J. Am. Chem. Soc.* 2002; **124**: 2428.
22. Freunscht P, Van Duyne RP, Schneider S. *Chem. Phys. Lett.* 1997; **281**: 372.
23. Tian ZQ, Ren B, Wu DY. *J. Phys. Chem. B.* 2002; **106**: 9463.
24. Van Duyne RP, Haushalter JP. *J. Phys. Chem.* 1983; **87**: 2999.
25. Van Duyne RP, Haushalter JP, Janik-Czachor M, Levinger N. *J. Phys. Chem.* 1985; **89**: 4055.
26. Van Duyne RP, Janik-Czachor M. *J. Electrochem. Soc.* 1983; **130**: 2320.
27. Hayazawa N, Inouye Y, Sekkat Z, Kawata S. *J. Chem. Phys.* 2002; **117**: 1296.
28. Van Duyne RP. *Laser Excitation of Raman Scattering from Adsorbed Molecules on Electrode Surfaces*, vol. 4. Academic Press: New York, 1979; 101.
29. Fleischmann M, Hendra PJ, McQuillan AJ. *Chem. Phys. Lett.* 1974; **26**: 163.
30. Van Duyne RP. *J. Phys.* 1977; **38**: (C5)239.
31. Van Duyne RP, Jeanmaire DL, Suchanski MR, Wallace WL, Cape TW. *149th National Meeting of the Electrochemical Society*, 1976; abstract no. 357.
32. Fussa-Rydel O, Zhang H-T, Hupp JT, Leidner CR. *Inorg. Chem.* 1988; **28**: 1533.
33. Bailey GF, Karp S, Sacks LE. *J. Bacteriol.* 1965; **89**: 984.
34. Palegrosdemange C, Simon ES, Prime KL, Whitesides GM. *J. Am. Chem. Soc.* 1991; **113**: 12.
35. Malinsky MD, Kelly KL, Schatz GC, Van Duyne RP. *J. Am. Chem. Soc.* 2001; **123**: 1471.
36. Liao PF, Bergman JG, Chemla DS, Wokaun A, Melngailis J, Hawryluk AM, Economou NP. *Chem. Phys. Lett.* 1981; **81**: 355.
37. Gregory BW, Clark BK, Standard JM, Avila A. *J. Phys. Chem. B.* 2001; **105**: 4684.
38. Otto A, Mrozek I, Grabhorn H, Akemann W. *J. Phys. Condens. Matter.* 1992; **4**: 1143.
39. Haynes CL, Van Duyne RP. *J. Phys. Chem. B.* 2001; **105**: 5599.
40. Jensen TR, Duval Malinsky M, Haynes CL, Van Duyne RP. *J. Phys. Chem. B.* 2000; **104**: 10 549.
41. Nie S, Emory SR. *Science.* 1997; **275**: 1102.
42. Kneipp K, Wang Y, Kneipp H, Perelman LT, Itzkan I, Dasari RR, Feld MS. *Phys. Rev. Lett.* 1997; **78**: 1667.
43. Goodacre R, Shann B, Gilbert RJ, Timmins EM, McGovern AC, Alsberg BK, Kell DB, Logan NA. *Anal. Chem.* 2000; **72**: 119.
44. Jarvis MR, Goodacre R. *Anal. Chem.* 2004; **76**: 40.
45. Carmona P. *Spectrochim. Acta Part A* 1980; **36A**: 705.
46. Mosier-Boss PA, Lieberman SH. *Appl. Spectrosc.* 2000; **54**: 1126.
47. Farquharson S, Gift AD, Maksymiuk P, Inscore FE. *Appl. Spectrosc.* 2004; **58**: 351.
48. Chin JE. *Control of Communicable Diseases Manual*. American Public Health Association: Washington, DC, 2000; 20.
49. English RD, Warscheid B, Fenselau C, Cotter RJ. *Anal. Chem.* 2003; **75**: 6886.
50. McCreery RL. *Raman Spectroscopy for Chemical Analysis*, vol. 157; John Wiley: New York, 2000; 420.
51. Blanco Gomis D, Muro Tamayo J, Alonso M. *Anal. Chim. Acta* 2001; **436**: 173.
52. Carron KT, Kennedy BJ. *Anal. Chem.* 1995; **67**: 3353.
53. Yang L, Janle E, Huang T, Gitzen J, Kissinger PT, Vreeke M, Heller A. *Anal. Chem.* 1995; **34**: 1326.
54. Deschaines TO, Carron KT. *Appl. Spectrosc.* 1997; **51**: 1355.
55. Walczak MM, Chung C, Stole SM, Widrig CA, Porter MD. *J. Am. Chem. Soc.* 1991; **113**: 2370.
56. Ostuni E, Chapman RG, Liang MN, Meluleni G, Pier G, Ingber DE, Whitesides GM. *Langmuir* 2001; **17**: 6336.
57. Lahiri J, Isaacs L, Tien J, Whitesides GM. *Anal. Chem.* 1999; **71**: 777.
58. Clark SL, Hammond PT. *Adv. Mater.* 1998; **10**: 1515.
59. Prime KL, Whitesides GM. *J. Am. Chem. Soc.* 1993; **115**: 10 714.
60. Mauzac MAN, Jozefonvicz J. *Biomaterials* 1982; **3**: 221.
61. Lee JH, Kopecek J, Andrade JD. *J. Biomed. Mater. Res.* 1989; **23**: 351.
62. Clarke WL, Cox D, Gonder-Frederick LA, Carter W, Pohl SL. *Diabetes Care* 1987; **10**: 622.